EFFECTS OF SOOT DEPOSITION AND SLOT EROSION ON THE MIST FILM-COOLING OF A FLAT PLATE IN THE PRESENCE OF UPSTREAM RAMP

Mr. Jishnu Handique

Junior Research Fellow,

Indian Institute of Technology Kharagpur,

West Bengal -721302 (**India**)

Dr. Kuldeep Singh*

*Corresponding author,

Senior CFD Research Fellow

Gas Turbine and Transmissions Research Centre

Nottingham University- NG7 2TU (**United Kingdom)**.

Email ID: kuldeep.singh@nottingham.ac.uk

Dr. Dushyant Singh*

*Corresponding author,

Assistant Professor,

Department of Mechanical Engineering,

National Institute of Technology, Manipur

Imphal, Manipur **– 795004 (India)**

Email ID: dushyant7raghu@gamil.com & dushyant@nitmanipur.ac.in

Abstract

In the present work, the numerical analysis is conducted on the film cooling of a flat plate with the air and mist injection from a slot. The effect of soot deposition and erosion of the cooling slot has been investigated in the presence of an upstream ramp. Simulations are performed at blowing ratios, M = 1, 1.5 and 2 with the slot angles, θ = 30º, 45º and 60º. The effect of presence of upstream ramp is studied by varying ramp angles from α = 5º to 15º. The numerical study is carried out on Eulerian-Eulerian framework. Thermal phase change model based on the evaporation and condensation is used to account heat and mass transfer. It is found that the film cooling effectiveness is better for the mist injection as compared to the air injection. Soot deposition on the cooling slot has a significant influence on the film cooling effectiveness. The soot deposition is not always adversely affecting the film cooling effectiveness. Moreover, the film cooling effectiveness decreases for the eroded slot for all the investigated slot angles and ramp angles for mist injection. An increment in the film cooling effectiveness is observed for $0 < x/2w < 15$ in the presence of the upstream ramp thereafter film cooling decreases as compared to the case without the upstream ramp. The optimum slot angle to inject the mist is found to be θ = 45º for the slot deposition.

Keywords: Mist Injection, Film cooling, Soot deposition, Erosion, Multiphase Flow

Nomenclature

A_x	Interfacial surface area per unit volume
B	Length of deposition and erosion
C	Coolant
d_o	Droplet diameter
DL	Downstream deposition location
E-DL	Downstream erosion location
g	Acceleration due to gravity
h	Height of deposition and erosion
h^E	Specific enthalpy
h'	Heat transfer coefficient
k	Turbulent kinetic energy
L	Slot length
M	Blowing ratio
$\dot{m}$	Mass flow rate

p	Pressure
Q	Interphase heat transfer
R	Interphase interaction force
T_C	Coolant temperature
T_{MS}	Mainstream temperature
T_P	Plate temperature
UL	Upstream deposition location
$\vec{U}$	Velocity vector
U_{MS}	Mainstream velocity
U_C	Coolant velocity
w	Slot width

Greek letters

α	Upstream ramp angle
β	Volume fraction
Ɛ	Turbulence dissipation rate
η	Effectiveness of film cooling
θ	Slot angle
μ	Phase viscosity
μ_T	Turbulence viscosity
ρ	Phase density
$\bar{\bar{\tau}}$	Strain tensor
ϕ	Mist loading fraction
ω	Non-dimensional temperature ($\frac{T_{MS}-T_C}{T_{MS}-T_P}$)

Subscripts and Superscripts

i, j	Phase subscript

1 Introduction

Film Cooling is a technique that is broadly used in gas turbine applications. This technique is used to cool the gas turbine blades and its different components that directly come in contact with the hot gas. In this process, a coolant is injected through a secondary hole. The coolant will form a low-temperature film above the surface of the component. The film resists the heat transfer from the hot

gas and protects the component surface. This process has been examined for many years, and this is still active research in the field of gas turbine cooling [1,2].

The performance of film cooling is mainly dependent on blowing ratio, density ratio, injection angle, hole geometry etc. However, the researchers are using new techniques to improve film cooling effectiveness. Many researchers [3-9] performed the experimental works on this technique. Similarly, a number of numerical studies [10-12] can also be found for the effects of different parameters on the air film cooling. Jia et. al [13] studied the film cooling process for slotted jet into a crossflow with LDV experiment as well as numerical simulation. The V^2f turbulence model was used in the numerical study. They varied the jet angles and blowing ratios from 15º to 90º and 2 to 9 respectively. Recirculation was observed for jet angles larger than 40º in their investigation. In addition, they found that variation of blowing ratio largely affects the film cooling effectiveness and it is highest for the jet angle 30º. Singh et. al [14,15] conducted the numerical analysis on the film cooling effectiveness with different blowing ratios, density ratios, and injection angles. They used the slotted hole on a 2D flat plate and a corrugated surface. Ely et. al [16] and Khajehhasani et. al [17] discussed the novel sister hole in air film cooling. They reported that the technique notably improves the film cooling performance.

Along with the single-phase air film cooling study, numerous works can also be found for mist film cooling. Jiang et al. [18,19] analyzed the effects of mist concentration, droplet size, and particle wall interaction conditions on the improvement of cooling performance. Li and Wang [20] presented a computational work on film cooling effectiveness by air and mist injection over a flat plate. In this paper, they studied for a 2D slotted hole coupled with 3D round and fan-shaped holes. The DPM results showed that the addition of water droplets in air injection can improve effectiveness. In the slotted hole, the mist film cooling performs better for lower droplet size with a high concentration of water. Again, the 2D cases explained that the lower the blowing ratio, the greater the mist effectiveness. The authors later examined the effects of various modeling, surface curvature, conjugate heat transfer and engine operating conditions with high temperature and pressure on mist film cooling performance [21-24].

The flow obstruction by the deposition also plays an important role in the film cooling performance. Sundaram and Thole [25] evaluated the influence of surface deposition and hole blockage on a large-scale turbine blade cascade. They illustrated that occurrence of deposition near the hole exit can enhance the effectiveness at the leading edge. But the increase in the deposition height leads to lower performance of the cooling process. Wang et.al [26,27,28] investigated the effects of deposition locations as well as height and width for air and mist injection. The authors found that for air injection, deposition location moving away from the hole worsens the cooling effectiveness

on the surface deposition. But the performance between the hole and deposition is increased significantly. In the mist cases, the effectiveness is better for the deposition located in the middle. The cooling performance is enhanced at the downstream of deposition as water droplets fly downstream the wall. Additionally, by decreasing the height of deposition and the blowing ratio, the film cooling performance can be increased. Subsequently, Wang et. al [29] presented a numerical work on mist film cooling with deposition by using different boundary conditions and droplet sizes. Kistenmacher et al. [30] studied the effect of contaminant deposition and found that the unmitigated deposition results in some additional thermal insulation. It causes an increase in the overall cooling effectiveness for round holes.

The researchers recently found that the upstream ramp plays an important role in film cooling performance. Na and Shih [31] investigated the adiabatic film cooling effectiveness using an upstream ramp. They used ramp angle ranging from 8.5º to 14º and the blowing ratios of 0.36, 0.49, 0.56 and 0.98. Results showed that the surface heat transfer is greatly reduced due to ramp. But the laterally averaged adiabatic effectiveness with the ramp was found to be two or more times higher than that of without ramp. Also, the optimal ramp shape relies on the blowing ratio. Chen et. al [32] experimentally studied the local film cooling effectiveness and heat transfer coefficient with an upstream ramp. They reported that the cooling performance at the downstream of the hole is dependent on the ramp height coupled with the blowing ratio. Rallabandi et. al [33] conducted a similar experiment with various hole geometries using the PSP technique. Abdala and his colleagues [34,35] presented the numerical investigations with various upstream ramp geometries. Velocity profiles and pressure coefficient profiles were discussed in their paper. Also, they analyzed the effectiveness and thermal contours for various blowing ratios. A higher lateral film cooling effectiveness and a lower heat transfer coefficient were observed for a curved step compared to a normal step.

The above literature revealed that along with the other parameters, film cooling effectiveness depends on the flow interaction with deposition as well as the ramp. Again, the continuous injection of water droplets in the mist film cooling process may erode the wall of the secondary hole. Hence the study on the effect of erosion is also very essential in case of mist injection. To best of our knowledge, the researchers never investigated the effects of deposition as well as erosion inside the secondary hole. In the present study, the effects of deposition and erosion locations inside a slotted hole combined with ramps were investigated for air and mist injection. The influence of the blowing ratio and slot angle was also reported.

2. Problem Formulation

The present study was carried out for the 2D geometries with secondary slots to investigate the two-phase problem. A transient and turbulent flow was considered for this study. The hot gas was passed through the mainstream inlet and the air-water mist was injected as coolant through the secondary slot. The plate was ramped at the angles of 5º, 10º and 15º. The analysis was conducted for blowing ratio, M = 1, 1.5 and 2. The coolant was injected at 300 K while the hot gas flew at 600 K. The effect of slot angles on effectiveness was also evaluated for θ = 30º, 45º and 60º. Fig. 1 (a) represents the computational domain of the problem. The slot width, w was considered as 4 mm. The length and height of the numerical domain were 80w and 20w respectively.

The depositions and erosions were located at various locations inside the slot. The slot length, L = 5w. The length of the depositions or, erosions, b was maintained as L/10; while the height of the depositions or, depth of the erosions, h was set to w/5. The configurations and the locations of the deposition as well as erosion are shown in Fig. 1 (b)-(d). A detail of various locations of deposition and erosion can also be found in Table-1.

In the present numerical analysis, the mist loading fraction is calculated as:

$$f = \frac{\dot{m}_W}{\dot{m}_A}$$

Where $\dot{m}_W$ is the mass flux of water, while $\dot{m}_A$ is the mass flux of air. Therefore, the mist loading fraction is defined as the ratio of water mass flux to the air mass flux that is considered for the mist coolant injection [36].

The film cooling effectiveness or performance is expressed as:

$$\eta = \frac{T_{MS} - T_P}{T_{MS} - T_C}$$

The blowing ratio, M defines how much coolant mass flux will be injected corresponding to the mainstream mass flux [14].

$$M = \frac{\rho_C \times U_C}{\rho_{MS} \times U_{MS}}$$

2.1. Mathematical model

Mathematical Formulations for Phase Continuity, Momentum, and Energy transfer can be described as follows:

Continuty equation for phase *j*:

$$\frac{\partial(\beta_j \rho_j)}{\partial t} + \nabla.(\beta_j \rho_j \vec{U}_j) = \dot{m}_{ij} - \dot{m}_{ji} + S_j \qquad (1)$$

In this study, the air is considered as the continuous or primary phase while water is taken as the secondary phase. In Eq. (1), β_j is the volume fraction of phase *j*. It defines the volume of phase *j* that

is considered in the total volume of the multiphase system. $\vec{U}_j$ is the velocity of phase *j*. The mass transfer from phase *i* to phase *j* and phase *j* to phase *i* are expressed by $\dot{m}_{ij}$and $\dot{m}_{ji}$ respectively. $S_j$is known as the mass source term which is the added mass to the phase *j* from the phase *i* (the droplets evaporation).

Momentum equation for phase *j*:

$$\frac{\partial(\beta_j\rho_j\vec{U}_j)}{\partial t} + \nabla.(\beta_j\rho_j\vec{U}_j\vec{U}_j) = -\beta_j\nabla p + \nabla.\bar{\bar{\tau}}_j + \beta_j\rho_j\vec{g} + \vec{R}_{ij} + \dot{m}_{ij}\vec{U}_{ij} - \dot{m}_{ji}\vec{U}_{ji} + \sum\vec{F}_j \quad (2)$$

Here $\bar{\bar{\tau}}_j$ is the strain tensor for the phase j. $\vec{R}_{ij} = -\vec{R}_{ji}$ denotes the interaction force between phases i and j. $\sum\vec{F}_j$ is the external body forces.

Energy conservation equation for phase j:

$$\frac{\partial(\beta_j\rho_j h^E{}_j)}{\partial t} + \nabla.(\beta_j\rho_j h^E{}_j\vec{U}_j) = \beta_j\frac{dp_j}{dt} + \nabla.\bar{\bar{\tau}}_j:\nabla\vec{U}_j - \nabla\vec{q}_j + Y_j + Q_{ij} + \dot{m}_{ij}h^E{}_{ij} - \dot{m}_{ji}h^E{}_{ji} \quad (3)$$

In the energy conservation equation the specific enthalpy, heat flux and enthalpy sources for phase j can be represented by $h^E{}_j$, $\vec{q}_j$ and Y_j respectively. $h^E{}_{ij}$is the enthalpy between the both phases. The interphase heat exchange intensity can be obtained from $Q_{ij} = -Q_{ji}$

The phase transformation was modelled with the thermal phase change model. According to this model, the mass transfer occurs between the phases based on the interphase heat transfer.

$$Q_{ij} + Q_{ji} = 0 \quad (4)$$

The heat transfer from the interphase to the phase j can be calculated by,

$$Q_{ij} = h'_{ij}A_x(T_{sat} - T_j) + \dot{m}_{ij}H_{js} \quad (5)$$

The saturation temperature T_{sat} is considered as the same on both sides of the interface.

The heat transfer from the interphase to the phase i can be calculated by,

$$Q_{ji} = h'_{ji}A_x(T_{sat} - T_i) - \dot{m}_{ij}H_{is} \quad (6)$$

The mass transfer between the phases is expressed as,

$$\dot{m}_{ij} = -\left[\frac{h'_{ij}A_x(T_{sat} - T_j) + h'_{ji}A_x(T_{sat} - T_i)}{H_{js} - H_{is}}\right] \quad (7)$$

The heat transfer coefficient for phase j and i are denoted as h'_{ij} and h'_{ji} respectively. Again, H_{js} and H_{is} are known as the enthalpies for phase j and i respectively. And, the interfacial surface area per unit volume, A_x found in the above equation can be represented by,

$$A_x = \frac{6\beta_i}{d_o} \tag{8}$$

d_o is the droplet diameter for the phase i.

Evaporation takes place for $\dot{m}_{ij} \geq 0$,

Then, $H_{is} = H_i(T_i)$

$H_{js} = H_j(T_{sat})$

Condensation takes place for $\dot{m}_{ij} < 0$,

Then, $H_{js} = H_j(T_j)$

$H_{is} = H_i(T_{sat})$

The latent heat of evaporation, $h_{ij} = H_j(T_{sat}) - H_i(T_{sat})$ (9)

Where H_i and H_j are the total phase enthalpies for phase i and j respectively. An explanation on the above equations can be found in [37].

In the present study, the standard $k - \varepsilon$ turbulence model proposed by Launder and Splading [38] was considered as it has been found to be better for the film cooling study on a flat plate. The transport equation for k and ε are as follows [38].

$$\frac{\partial(\beta_j \rho_j k_j)}{\partial t} + \nabla.(\beta_j \rho_j k_j \vec{U}_j) = \nabla.(\psi_j(\mu_j + \frac{\mu_{T,j}}{Pr_k})\nabla k_j) + \beta_j G_{k,j} - \beta_j \rho_j \varepsilon_j + S_k \tag{10}$$

$$\frac{\partial(\beta_j \rho_j \varepsilon_j)}{\partial t} + \nabla.(\beta_j \rho_j \varepsilon_j \vec{U}_j) = \nabla.(\beta_j(\mu_j + \frac{\mu_{T,j}}{Pr_\varepsilon})\nabla \varepsilon_j) + \beta_j C_a \frac{\varepsilon_j}{k_j} G_{k,j} - \beta_j C_b \rho_j \frac{\varepsilon_j^2}{k_j} + S_\varepsilon \tag{11}$$

Where turbulent viscosity can be defined as:

$$\mu_{T,j} = \rho_j C_\mu \frac{k_j^2}{\varepsilon_j} \tag{12}$$

$G_{k,j}$ is known as turbulence production term.Pr_k and Pr_ε expresses the turbulent Prandtl numbers for the turbulent kinetic energy and turbulence dissipation rates respectively. S_k and $S_\varepsilon$denote the source terms due to phase interaction. The model constants involved in the Eq. (10) and (11) are considered as C_a = 1.44, C_b = 1.92 and C_μ = 0.09.

2.2. Solution Procedure and Boundary Conditions

The geometries and meshes were generated using commercial Ansys software package ICEM CFD. The meshes were later imported to the opensource CFD software OpenFOAM, and analyses were carried out with an Eulerian-Eulerian multiphase solver. The standard k-ε model was used for the turbulence. The thermal phase change model was introduced for the phase transformation in the air-water multiphase system. The pressure and velocity coupling were solved by the PIMPLE algorithm which combines the PISO and SIMPLE algorithm. The convective and turbulent terms were discretized by the Gauss Upwind technique [39]. The temporal term was discretized using the Implicit Eulerian scheme. The boundary conditions used in the present analysis are given in the Table-2.

2.3. Mesh Sensitivity Study

The grid sensitivity test was performed for ϕ = 2% and $\alpha = 15^0$ and θ was kept at 30º with the deposition at DL = 0. Three different grid sizes having quadrilateral cells 178×80 (Mesh 1), 220×96 (Mesh 2) and 268×116 (Mesh 3) were studied and presented in Fig. 2 (b). The mainstream gas was passed at 600 K and the blowing ratio was maintained as 1. Mesh near the walls were made fine to ensure the optimum Y+ value. The effectiveness of the mist film cooling was studied on the plate surface. The result of the low grid sized model shows a large deviation from that of the other models. But there are negligible differences between the outcomes of higher cell-sized models. Hence, the medium grid sized model (having average grid spacing, $x = 1.317\times10^{-3}$ m and $y = 1.0996\times10^{-3}$ m) was considered for the further numerical study.

2.4. Validation

Due to the lack of the availability of the experimental result on the slot mist film cooling study over a flat plate; the present numerical work is validated against the benchmark experimental data [40] and numerical works [14,41] of air film cooling for the slot angle, $\theta = 90^o$ and blowing ratio, M = 1. The comparison of air film cooling effectiveness is shown in Fig. 3. It can be observed that air film cooling performane obtained from the present numerical work matches well with the experimental as well earlier numerical works. A comparison of non-dimensional horizontal velocity obtained from the present numerical study with the benchmark experimental data [42] and numerical works [12,14,43] for the slot angle, $\theta = 90^o$ and blowing ratio, M = 0.8 is shown in Fig.4. It can be noticed that the present numerical result is in the good agreement with the benchmark experimental and numerical results.

The validation study of air-water mist film cooling is performed for mist loading fraction, ϕ = 2%, coolant injection angle, $\theta = 35^o$ and blowing ratio, M = 1. Fig. 5 (a) shows the comparison of mist film cooling effectiveness along the non-dimenosinal plate length obtained in the present numerical study and previous numerical data available in the literature [20]. Figure 5 (b) represents the

comparison of temperature variations along the height of the domain obtained from the present analysis and the numerical data [20]. A very good agreement of the present numerical results with the benchmark test case can be observed in Fig. 5 (a) as well as Fig. 5 (b). Thus, the numerical methodology is capable to predict film cooling performance with air and mist injection and can be used further for the parametric studies.

3. Results and Discussion

The present numerical study is carried out to distinguish the effects of the parameters namely, the locations of depositions and erosions, ramp angle, slot angle and blowing ratio on film cooling effectiveness. The range of parameters investigated in this study is given in Table-3.

3.1. Studies with Depositions

3.1.1. Effect of Mist Injection on Film-Cooling

The effect of mist injection on the film cooling performance is presented in Fig. 6 for the cooling slot without blockage and slot blockage at DL0 and UL0 location. Film cooling effectiveness in the vicinity of the cooling slot ($x/2w < 5$) is almost comparable for air and mist injection. However, a significant impact of mist injection can be observed on the film cooling effectiveness downstream of the cooling slot ($5 < x/2w < 30$) for unblocked slot. The merit of mist injection is compromised for blocked slot DL0. For this geometric configuration, film cooling for air and mist injection is identical for downstream distance $x/2w < 15$ thereafter mist film cooling is found to be better than the air injection. Moreover, the mist film cooling effectiveness for slot blockage UL0 is better than the air injection.

The contours of volume fraction of water are presented in Fig. 7 for two slot blockage configurations, DL0 and UL0. It can be observed from this figure that the water volume fraction on the target plate is higher for $x/2w > 5$. This eventually increases cooling effectiveness downstream of the slot for mist injection. It can also be observed that the vapour concentration at slot deposition DL0 is higher as compared to UL0 location.

3.1.2. Effect of Deposition on Film-Cooling

The effect of slot blockage due to soot deposition inside the cooling slot at three upstream and three downstream locations is presented in Fig. 8. In order to identify the impact of deposition location, the film cooling effectiveness is normalized with the film cooling effectiveness of unblocked slot. The film cooling effectiveness of air injection is normalized with the unblocked slot air injection case. Similarly, the film cooling effectiveness of mist injection is normalized with the unblocked slot mist injection case. Thus, the ratio $\eta/\eta_{Baseline} = 1$ represents the same cooling effectiveness with the

blockage slot as that of the baseline case without blockage. The increment ($\eta/\eta_{Baseline} > 1$) or the decrement ($\eta/\eta_{Baseline} < 1$) in the film cooling effectiveness is distinguished by this ratio. It can be observed from Fig. 8 (a) that the film cooling performance at all the downstream deposition location-DL0 improves significantly for the air injection. A marginal increment in the film cooling effectiveness is also observed for DL0.5 and DL1 locations. Although increment in the film cooling effectiveness is observed for mist injection for DL0 location, as can be seen in Fig. 8 (b). However, this increment is not as significant as that found for the air injection. This explains, why enhancement in film cooling due to mist injection is not significant for DL0 location as reported in the previous section, refer Fig. 6 (b). A slight decrement in the film cooling effectiveness is observed for DL0.5 and DL1 location for mist injection.

Film cooling effectiveness decreases for the slot blockage on the upstream side for both air and mist injection. A noticeable decrement in the film cooling effectiveness is observed for cooling slot blockage at UL1 location. The reason behind this is the recirculation of coolant flow occurs inside the cooling slot due to blockage at UL1 as can be seen in Fig.9. A higher concentration of water on the slot walls is also observed for slot blockage at UL1. This reduces the potential of cooling in the case of mist injection.

3.1.3. Effect of Upstream Ramp Angle on Film-Cooling

The presence of the upstream ramp influences the interaction of mainstream air with the coolant jet. The effect of the upstream ramp is analyzed for three ramp angles: $\alpha = 5^o$, 10^o and 15^o for both air injection and mist injection. The film cooling effectiveness is normalized with the cooling effectiveness for the case without a ramp and presented in Fig. 10. It can be observed from Fig. 10 that the film cooling effectiveness increases because of the ramp configuration upto $x/2w < 15$ and thereafter starts decreasing. A maximum gain of 2% in the film cooling effectiveness is observed for the ramp angle of 10^o with air and mist injection. It can be noticed from Fig. 11 that the ramping of the plate allows the shear layer separation and creates a low-pressure zone just downstream of the ramp. It causes the flow recirculation at the immediate downstream of the ramp. As a consequence the water content is trapped in the recirculation zone. Thus it increases the turbulence as shown in Fig. 11. This turbulent shear layer prevents the coolant from the lift-off when it comes out of the slot exit. Simply, the turbulent recirculation reattaches the coolant upto a distance. Therefore, an increment in the cooling performance can be observed till $x/2w = 15$. Since the rise in turbulent kinetic energy is also responsible for an increase in the mixing of the coolant with mainstream fluid, a less amount of the coolant will remain attached to the plate. It weakens the film layer protection and hence, the performance starts to decrease afterward.

3.1.4. Combined Effect of Hole Blockage and Ramp Angle

The effects of deposition and upstream ramp on the film cooling performance are discussed individually in the previous sections. The effect of hole deposition is investigated in the presence of the upstream ramp and presented in this section. The mist film cooling performance is analyzed for downstream locations DL0, DL0.5, DL1; and upstream locations UL0, UL0.5, UL1 along with upstream ramp angle, $\alpha = 10^o$ and presented in Fig. 12. For the investigated configuration, film cooling effectiveness of DL0 location is better than that of DL0.5 and DL1 as shown in Fig. 12 (a). Among the upstream blockages, blockage at UL1 location decreases film cooling effectiveness at a faster rate as compared to UL0 and UL0.5. As mentioned in section 3.1.2, the upstream location UL1 creates recirculation inside the slot which forms a weaker film over the plate. Hence, UL0 and UL0.5 show better cooling effectiveness than that of UL1.

In the presence of the ramp, flow circulation is affected just upstream of the cooling slot. A recirculation region is formed because of the ramp as can be seen in Fig. 13. The cooling mist is trapped in this zone which eventually decreases the cooling effectiveness. It can be seen in Fig. 13 that the water content trapped in the recirculation zone is affected by the location of the deposition. The water content in this zone is least for DL0 configuration as compared to DL0.5 and DL1. Hence, the cooling effectiveness is better for deposition at DL0 location among the investigated locations.

3.1.5. Effect of Slot Angle

The slot angle has a predominant effect on the trajectory of the coolant into mainstream. The three slot angles, $\theta = 30^o$, 45^o and 60^o are studied in the presence of ramp angle, $\alpha = 10^o$ and downstream deposition, DL0. The effects of the coolant injection angle or slot angle are shown in Fig. 14. It can be observed that the film cooling effectiveness for all the investigated injection angle is identical near the cooling slot i.e. $0 < x/2w < 5$. Further, downstream film cooling effectiveness for the injection angle, $\theta = 45^o$ is better than the other injection angles. It can also be noticed that the film cooling effectiveness for injection angle $\theta = 60^o$ is better than that of $\theta = 30^o$ for downstream locations $x/2w > 18$. The flow trajectory of the secondary fluid and coolant distribution on the plate can be observed in Fig. 15. The coolant penetration in the mainstream is found to be least for the injection angle, $\theta = 30^o$. It can also be noticed that despite of slight increased penetration for $\theta = 45^o$, coolant coverage is better than that of $\theta = 30^o$ injection angle. Consequently, film cooling effectiveness for $\theta = 45^o$ is better than that of $\theta = 30^o$ injection angle. Moreover, coolant penetration into mainstream is maximum for 60^o injection angle among the investigated injection angle. A recirculation region just downstream ($x/2w < 1.8$) of the slot injection is observed for this injection angle. The coolant reattaches the surface due to impact of the mainstream. Hence, film cooling effectiveness is better for far downstream region i.e. $x/2w > 18$ for the injection angle of 60^o as compared to the injection angle

of 30º. This behaviour is of particular interest when small injection angle is prohibitive due to the thinner cross section of the film cooled surface i.e. for the lower hole length-to-diameter cases. The combustion chamber and after-burner liner are thinner as compared to the turbine blades. Shallow injection angle are not so effective for these geomteries.

3.1.6. Effect of Blowing Ratio

The cooling performance of a film cooling technique is dependent on blowing ratio. Blowing ratio is defined as the ratio of coolant mass flux to the mainstream mass flux. Hence, the mass flux of the coolant increases with a higher blowing ratio. A numerical analysis is performed for the blowing ratio, M = 1, 1.5 and 2 using a ramped plate. The mist film cooling performance is almost identical for the investigated blowing ratios in the region $0 < x/2w < 10$ as shown in Fig. 16. Thereafter, film cooling performance at M = 1.5 is found to be better. The mass of coolant injected onto the test plate increases with the increase in blowing ratio and hence film cooling effectiveness increases when blowing ratio is increased from M = 1 to M = 1.5. Moreover, increases in blowing ratio results in increased velocity of coolant. Consequently, penetration of cooling jet into mainstream increases and hence film cooling effectiveness decreases with further increases in blowing ratio to M = 2. It can also be observed that film cooling effectiveness of M = 2 is better than that of M = 1 for $20 < x/2w < 30$. This is because of the increased mass of coolant at higher blowing ratio.

3.2. Studies with Erosions

3.2.1 Comparison of Slot Erosion with Slot Deposition and Baseline Case

In order to investigate the effect of slot erosion on the film cooling effectiveness, numerical study is conducted by injecting air and mist without upstream ramp. The obtained film cooling effectiveness for deposition and erosion was normalized with the cooling effectiveness of the baseline case and presented in Fig. 17. The baseline case is the one in which there is no deposition or erosion and; keeping all other parameters the same. It can be observed from Fig. 17 that the film cooling effectiveness decreases because of the slot erosion for both air and mist injection. Decrement in the film cooling effectiveness because of the slot erosion is more prominent for mist injection. The film cooling effectiveness for the slot deposition increases as explained in the previous section (section 3.1).

The trajectory of the coolant ejection from the slot is altered because of the erosion as depicted in Fig. 18 by contours of non-dimensional velocity for air injection. It can be visualized that the ejection velocity increases for the deposition (DL0) and decreases for the erosion (E-DL0) case as compared with the velocity of the baseline case. The reason behind this is the deposition compacts the coolant exit slot while the erosion expands it. However, the velocity of the deposition case is higher,

it does not lead to a higher turbulence mixing as the coolant can proceed towards the plate without ramping. But due to the shape of erosion, the coolant penetrates and mixes with the mainstream fluid more than the baseline case. It leads to form a weaker coolant film and hence, causes a decrement in the film cooling performance as seen in Fig. 17.

3.2.2 Effect of Upstream Ramp Angle on Film-Cooling

Film cooling hole and slots are exposed to very high velocity. The presence of mist, soot particle can erode the cooling hole. In this section the effect of slot erosion on the cooling performance is presented. The impact of hole erosion at a location E-DL0 is studied in the presence of upstream ramp. The ramp angle was varied from 0º to 15º like the previous study with the slot deposition. The film cooling effectiveness obtained with the various ramp angle cases is normalized with that of without ramp and presented in Fig. 19. A distinct trend in film cooling effectiveness is observed for air cooling and mist cooling. Film cooling effectiveness for air injection increases upto $x/2w = 13$ for the investigated ramp angles and thereafter it starts decreasing. A maximum of 4% gain in the film cooling effectiveness is observed for the air injection. However, insignificant increment in the film cooling effectiveness is observed for mist injection in the region $0 < x/2w < 13$. The turbulent shear layer increases before the coolant exit due to the upstream ramp. It helps in the coolant attachment to the plate surface. Thus, the cooling performance increases till $x/2w = 13$ and thereafter it starts decreasing. The turbulent kinetic energy increases the fluid mixing which decreases the film protection.

3.2.3. Effect of Slot Angle

The coolant injection angle or slot angles, $\theta = 30º$, 45º and 60º are numerically analyzed for the case of downstream erosion, E-DL0 in the presence of ramp with $\alpha = 10º$ and presented in Fig. 20. The variation of film cooling effectiveness with the slot angle for the eroded slot follows the same trend as it was followed by deposition case. The film cooling effectiveness is best for $\theta = 45º$ among the investigated slot angle. The film cooling effectiveness for $\theta = 60º$ is lowest in the region $0 < x/2w < 18$ because of the higher penetration into the mainstream. However, reattachment of lifted-off jet for $\theta = 60º$ improves the film cooling effectiveness further downstream $18 < x/2w < 30$.

3.2.4. Effect of Blowing Ratio

The influence of blowing ratio on the film cooling effectiveness of eroded slot is investigated by varying blowing ratio from 1 to 2 in the presence of upstream ramp. An increment in the film cooling effectiveness is observed with the increase in the blowing ratio as can be seen in Fig. 21. As coolant mass increases with the increase in blowing ratio. Hence, availability of extra coolant improves film cooling effectiveness. This trend is different than the deposition case where optimum blowing ratio was 1.5. Unlike the slot deposition, erosion does not block the coolant flow. On the

other hand, it expands the coolant exit area which controls the momentum as well as the velocity of the coolant in the presence of ramp. The turbulence mixing is also controlled in the case of erosion and; it results in a better film cooling effectiveness with the higher blowing ratio.

4. Conclusions

In the current study, the effects on the film cooling effectiveness due to the locations of the deposition and erosion along with the upstream ramp, blowing ratios and slot angles were investigated. The following conclusions can be made from the present investigations:

(i) Film cooling effectiveness is better for the mist injection in comparison to the air injection. It is anticipated that the film cooling effectiveness will increases with the mist loading fraction up to saturation conditions. Moreover, increases in the droplet size may adversely affect the cooling performance as the bigger droplets are susceptible to the condensation.

(ii) Soot deposition on the cooling slot has a significant influence on the film cooling effectiveness. The soot deposition is not always adversely affecting the film cooling effectiveness. For soot depositon locations like DL0, enhancement in the film cooling effectiveness is observed for both mist and air-injection.

(iii) Presence of the upstream ramp influences the secondary flow emerged from the cooling slot. An increment in the film cooling effectiveness is observed for $0 < x/2w < 15$ in the presence of the upstream ramp thereafter film cooling decreases as compared to the case without the upstream ramp.

(iv) Slot erosion has adverse effect on the film cooling effectiveness. Film cooling effectiveness decreases for the eroded slot for all the investigated slot angles and ramp angles for mist injection.

(v) The optimum slot angle to inject the mist is found to be $\theta = 45^{o}$ for the slot deposition. At this injection angle, the coolant approaches more towards the plate in the presence of the upstream ramp. Similar results can also be found in the case of erosion.

References

1. Eriksen, V. L., Goldstein, R. J., Heat transfer and film cooling following injection through inclined tubes, ASME Journal of Heat Transfer, 1974, 96: 239–245.
2. Goldstein, R. J., Eckert, E. R. G., Burggraf, F., Effects of hole geometry and density on three-dimensional film cooling, International Journal of Heat Mass Transfer, 1974, 17: 595–607.
3. Wang, T., Chintalapati, S., Bunker, R.S., Lee, C.P., Jet mixing in a slot, Experimental Thermal and Fluid Science, 2000, 22(1-2): 1-17.
4. Metzger, D.E., Carper, H.J., Swank, L.R., Heat transfer film cooling near nontangential injection slots, ASME Journal of Engineering for Power, 1968, 90(2): 157-163.
5. Andreopoulos, J., Measurements in a jet-pipe flow issuing perpendicularly into a cross stream, Journal of Fluids Engineering, 1982, 104(4): 493-499.
6. Fitt, A.D., Ockendon, J.R., Jones, T.V., Aerodynamics of slot-film cooling: theory and experiment, Journal of Fluid Mechanics, 1985, 160: 15-30.
7. Teekaram, A.J.H., Forth, C.J.P., Jones, T.V., Film cooling in the presence of mainstream pressure gradients, ASME Journal of Turbomachinery, 1991, 113(3): 484-492.
8. Aly, S.E., Injection effect on two dimensional boundary layer, Energy Conversion and Management, 2000, 41(6): 539-550.
9. Cho, H.H., Ham, J.K., Influence of injection type and feed arrangement on flow and heat transfer in an injection slot, ASME Journal of Turbomachinery, 2002, 124(1): 132-141.
10. Bergeles, G., Gosman, A.D., Launder, B.E., The turbulent jet in a cross stream at low injection rates: a three dimensional numerical treatment, Numerical Heat Transfer A, 1978, 217-242.
11. Sarkar S., Bose, T.K., Comparison of different turbulence models for prediction of slot-film cooling-flow and temperaturefield, Numerical Heat Transfer B, 1995, 28(2): 217-238.
12. Kassimatis, P.G., Bergeles, G.C., Jones, T.V., Chew, J.W., Numerical investigation of the aerodynamics of the near slot film cooling, International Journal of Numerical Methods in Fluids, 2000, 32(1): 85-104.
13. Jia, R., Sunden, B., Miron, P., Leger, B., Numerical and experimental study of the slot film cooling jet with various angles, Proceedings of the ASME Summer Heat Transfer Conference, ASME, New York, 2003, 845–856.
14. Singh, K., Premachandran, B., Ravi, M.R., A numerical study on the 2d film cooling of a flat surface, Numerical Heat Transfer A, 2014, 67: 673–695.
15. Singh, K., Premachandran, B., Ravi, M.R., Numerical investigation of film cooling on a 2D corrugated surface, Numerical Heat Transfer A, 2016, 70(11): 1253-1270.

16. Ely, M.J., Jubran, B.A., A numerical study on improving large angle film cooling performance through the use of sister holes, Numerical Heat Transfer A, 2009, 55: 634–653.
17. Khajehhasani, S., Jubran, B.A., Numerical assessment of the film cooling through novel sister-shaped single-hole schemes, Numerical Heat Transfer A, 2015, 67: 414–435.
18. Jiang, Y., Zheng, Q., Dong, P., Zhang, H., Yu, F., Research on heavy-duty gas turbine vane high efficiency cooling performance considering coolant phase transfer, Applied Thermal Engineering, 2014, 73: 1175–1191.
19. Jiang, Y., Zheng, Q., Dong, P., Yue, G., Gao, J., Numerical simulation on turbine blade leading-edge high-efficiency film cooling by the application of water mist, Numerical Heat Transfer A, 2014, 66(12): 1341-1364.
20. Li, X., Wang, T., Simulation of film cooling enhancement with mist injection, ASME Journal of Heat Transfer, 2006, 128: 509–519.
21. Li, X., Wang, T., Effects of various modeling on mist film cooling, ASME Journal of Heat Transfer, 2007, 129: 472–482.
22. Li, X., Wang, T., Two-phase flow simulation of mist film cooling on turbine blades with conjugate internal cooling, ASME Journal of Heat Transfer, 2008, 130(10): 102901.
23. Li, X., Wang, T., Mist film cooling simulation at gas turbine operating conditions, International Journal of Heat and Mass Transfer, 2008, 51: 5305–5317.
24. Li, X., Wang, T., Computational analysis of surface curvature effect on mist film-cooling performance, ASME Journal of Heat Transfer, 2008, 130(12): 121901.
25. Sundaram, N., Thole, K.A., Effects of surface deposition, hole blockage, and thermal barrier coating spallation on vane endwall film cooling, ASME Journal of Turbomachinary, 2007, 129: 599–607.
26. Wang, J., Cui, P., Sunden, B., Yang, R., Effects of deposition locations on film cooling with and without a mist injection, Numerical Heat Transfer A, 2016, 70: 1072–1086.
27. Wang J., Cui P., Sunden B., Vujanović M., Effects of Deposition Height and Width on Film Cooling, Numerical Heat Transfer A, 2016, 70: 673–687.
28. Wang J., Cui P., Vujanović M., Baleta J., Duić N., Guzović Z., Effects of Surface Deposition and Droplet Injection on Film Cooling, Energy Conversion and Management, 2016, 125: 51–58.
29. Wang, J., Li, Q., Sundén, B., Baleta, J., Vujanović, M., Two-phase flow simulation of mist film cooling with deposition for various boundary conditions, Numerical Heat Transfer A, 2017, 71(9): 895-909.

30. Kistenmacher D. A., Davidson F. T., Bogard D. G., Realistic Trench Film Cooling with a Thermal Barrier Coating and Deposition, ASME Journal of Turbomachinary, 2014, 136: 091002.
31. Na, S., Shih, T.I.-P., Increasing adiabatic film-cooling effectiveness by using an upstream ramp, ASME Journal of Heat Transfer, 2007, 129: 464–471.
32. Chen, S.P., Chyu, M.K., Shih, T.I.-P., Effects of upstream ramp on the performance of film cooling, International Journal of Thermal Science, 2011, 50: 1085–1094.
33. Rallabandi, A.P., Grizzle, J., Han, J.C., Effect of upstream step on flat plate film cooling effectiveness using PSP, ASME Journal of Turbomachinary, 2011, 133: 041024.
34. Abdala, A.M., Elwekeel, F.N., An influence of novel upstream steps on film cooling performance, International Journal of Heat and Mass Transfer, 2016, 93: 86–96.
35. Abdala, A.M., Elwekeel, F.N., Huang, D.G., Film cooling effectiveness and flow structures for novel upstream step, Applied Thermal Engineering, 2016, 105: 397–410.
36. Khangembam, C., Singh, D., Handique, J., Singh, K., Experimental and numerical study of air-water mist jet impingement cooling on a cylinder, International Journal of Heat and Mass Transfer, 2020, 150: 119368.
37. Rane, S., He, L., CFD analysis of flashing flow in two-phase geothermal turbine design, Journal of Computational Design and Engineering, 2020, 7(2): 238-250.
38. Launder, B. E., Splading, D. B., The numerical computation of turbulent flows, Computer Methods in Applied Mechanics and Engineering, 1974, 3:269-289.
39. OpenFOAM v5 User Guide, 2017.
40. Papell, S. S., Effect on gaseous filmcooling injection through angled slots and normal holes, 1960, NASA TN-D-299:1-27.
41. Sarkar, S., Bose, T. K., Numerical simulation of a 2-d jet-cross flow interaction related to film cooling applications: effects of blowing rate, injection angle and free-stream turbulence, Sadhana, 1995, 20:915–935.
42. O'Malley, K., Theoretical aspects of film cooling, D.Phil. Thesis, University of Oxford, Oxford, 1984.
43. Bayraktar, S., Yilmaz, T., Two-dimensional numerical investigation of film cooling by a cool jet injected at various angles for different blowing ratios, Proceedings of the Institution of Mechanical Engineers Part C Journal of Mechanical Engineering Science, 2008, 222(7): 1215-1224.

Table-1: Locations of deposition and erosion considered in the present study.

Deposition/ Erosion / Position	**Upstream Deposition**	**Downstream Deposition**	**Downstream Erosion**
Top	UL0	DL0	E-DL0
Middle	UL0.5	DL0.5	E-DL0.5
Bottom	UL1	DL1	E-DL1

Table-2: Boundary conditions used in the present study.

Parameter	**Boundary Condition**
Main Stream and Secondary Stream Inlet	Constant Temperature and Velocity
Plate	Constant 0 Heat Flux and No Slip
Top Wall	Constant Temperature and No Slip
Slot Wall	Constant Temperature and No Slip
Outlet	Outflow

Table-3: Range of parameters investigated in the present study.

Parameter	**Value**
Mist loading fraction, ϕ	0, 2%
Droplet diameter, d_o	20 μm
Ramp angle, α	5º, 10º, 15º
Slot angle, θ	30º, 45º, 60º
Mainstream inlet velocity	10 m/sec
Mainstream temperature, T_{MS}	600 K
Secondary temperature, T_P	300 K
Saturation Temperature, T_{sat}	300 K
Blowing ratio, M	1, 1.5, 2

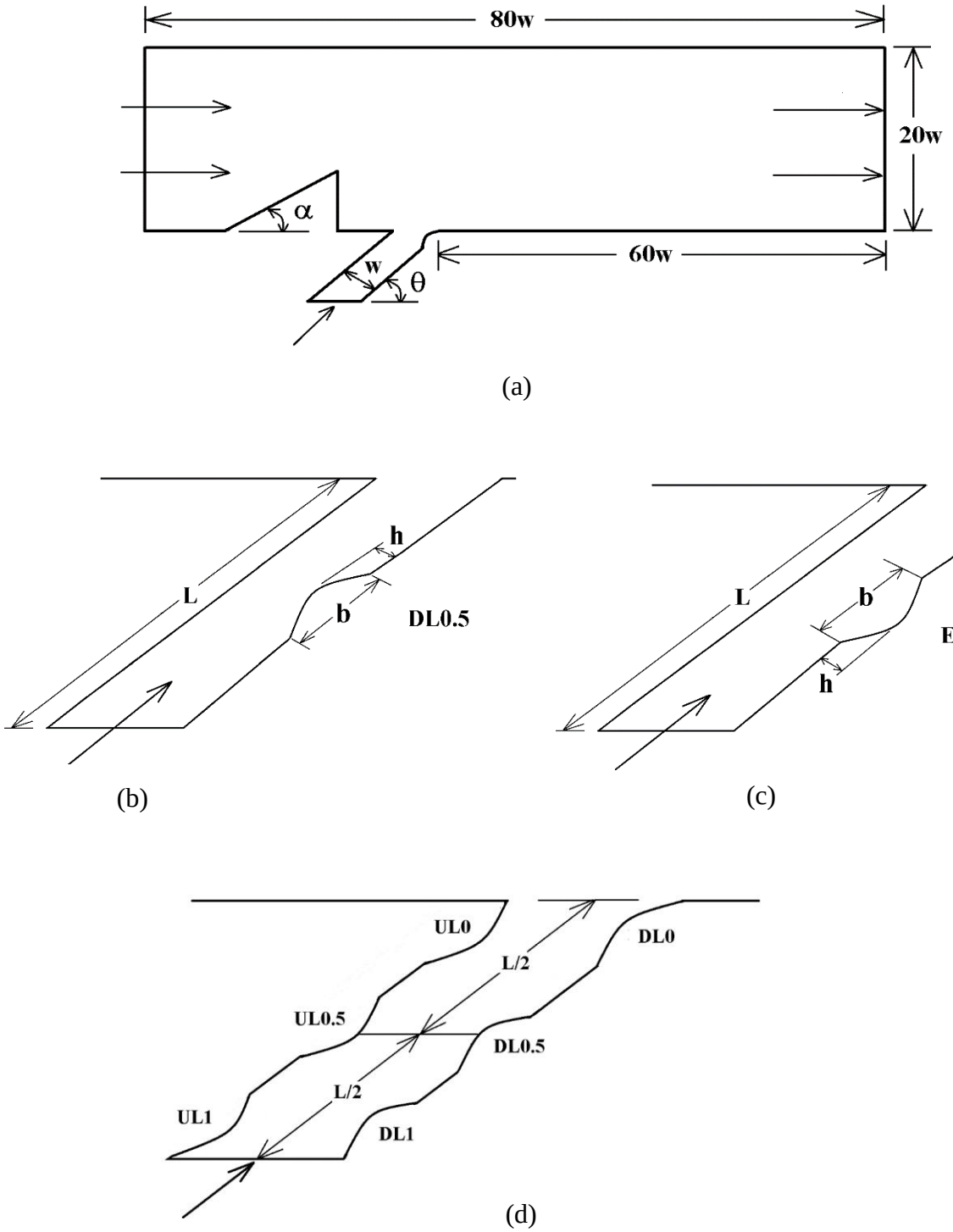

Figure 1. Schematic diagram of (a) numerical domain, (b) slot with deposition configuration (c) slot with erosion configuration (d) locations of deposition/erosion investigated in the present study.

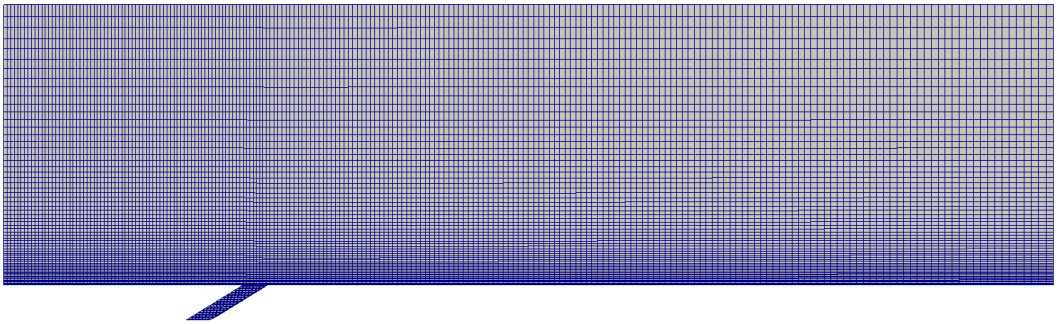

(a)

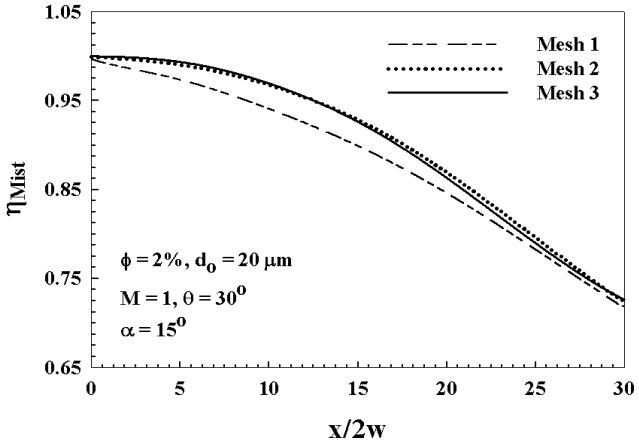

(b)

Figure 2. (a) Grid topology and (b) Grid independent numerical analysis

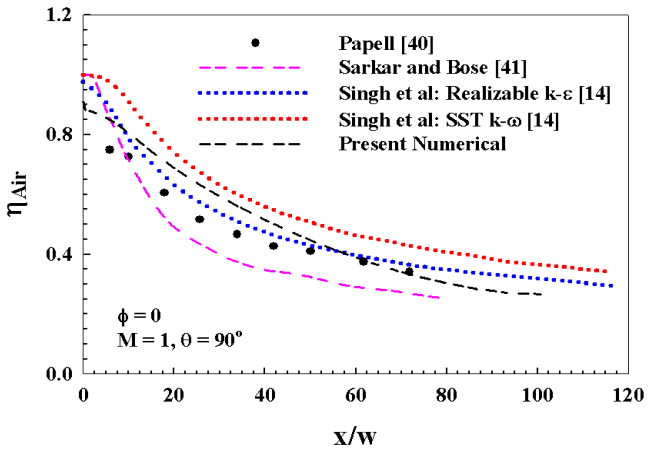

Figure 3. Validation of air film cooling results with the experimental data of Papell [40] and other published numerical data [14, 41].

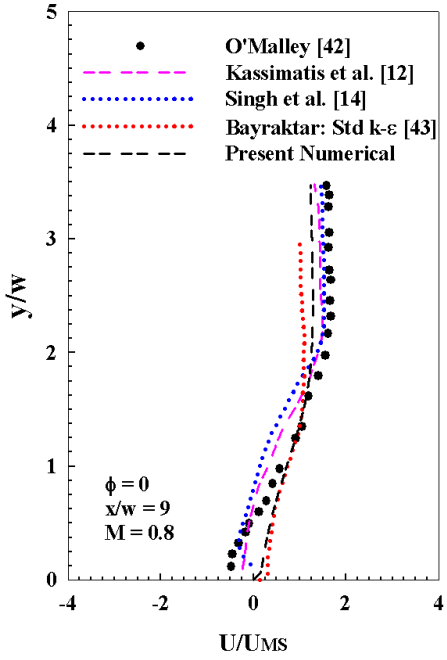

Figure 4. Comparison of non-dimensional horizontal velocity for air injection at x/w = 9 to the experimental results of O'Malley [42] and other published computational results [12, 14, 43].

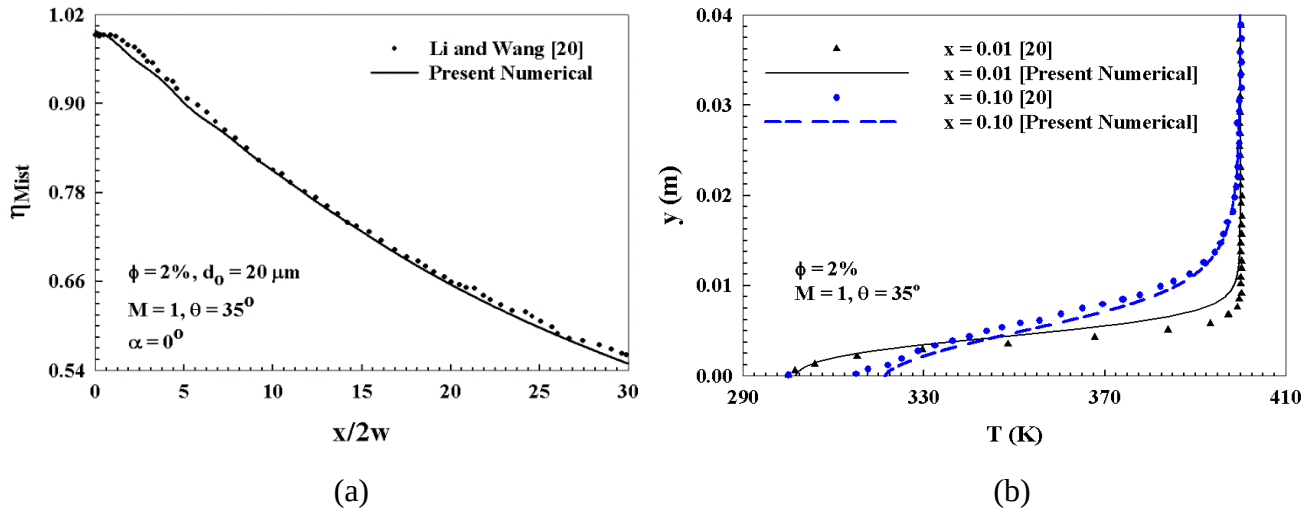

(a) (b)

Figure 5. Comparison of present (a) mist film cooling effectiveness and (b) temperature variations with the results of Li and Wang [20].

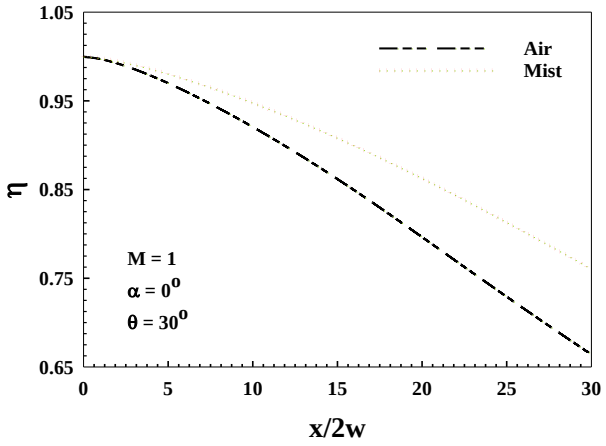

(a)

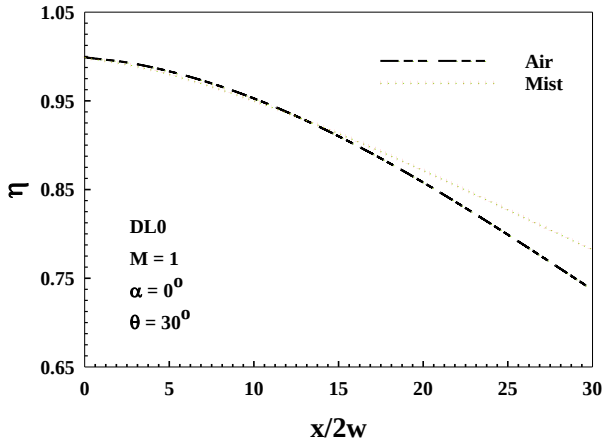

(b)

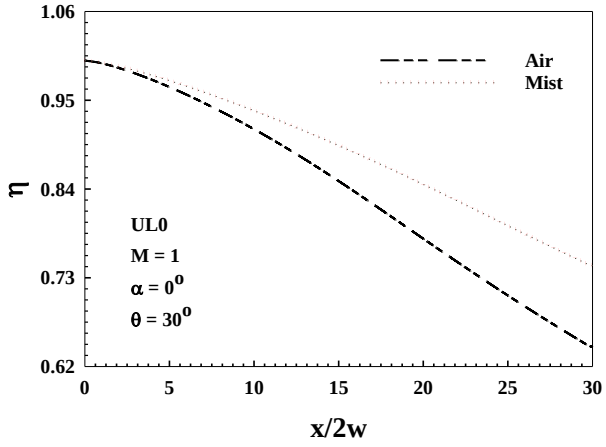

(c)

Figure 6. Comparison of film cooling effectiveness due to air and mist injection for M=1, α=0º and θ=30º, (a) without hole blockage (b) hole blockage at DL0 (c) hole blockage at UL0.

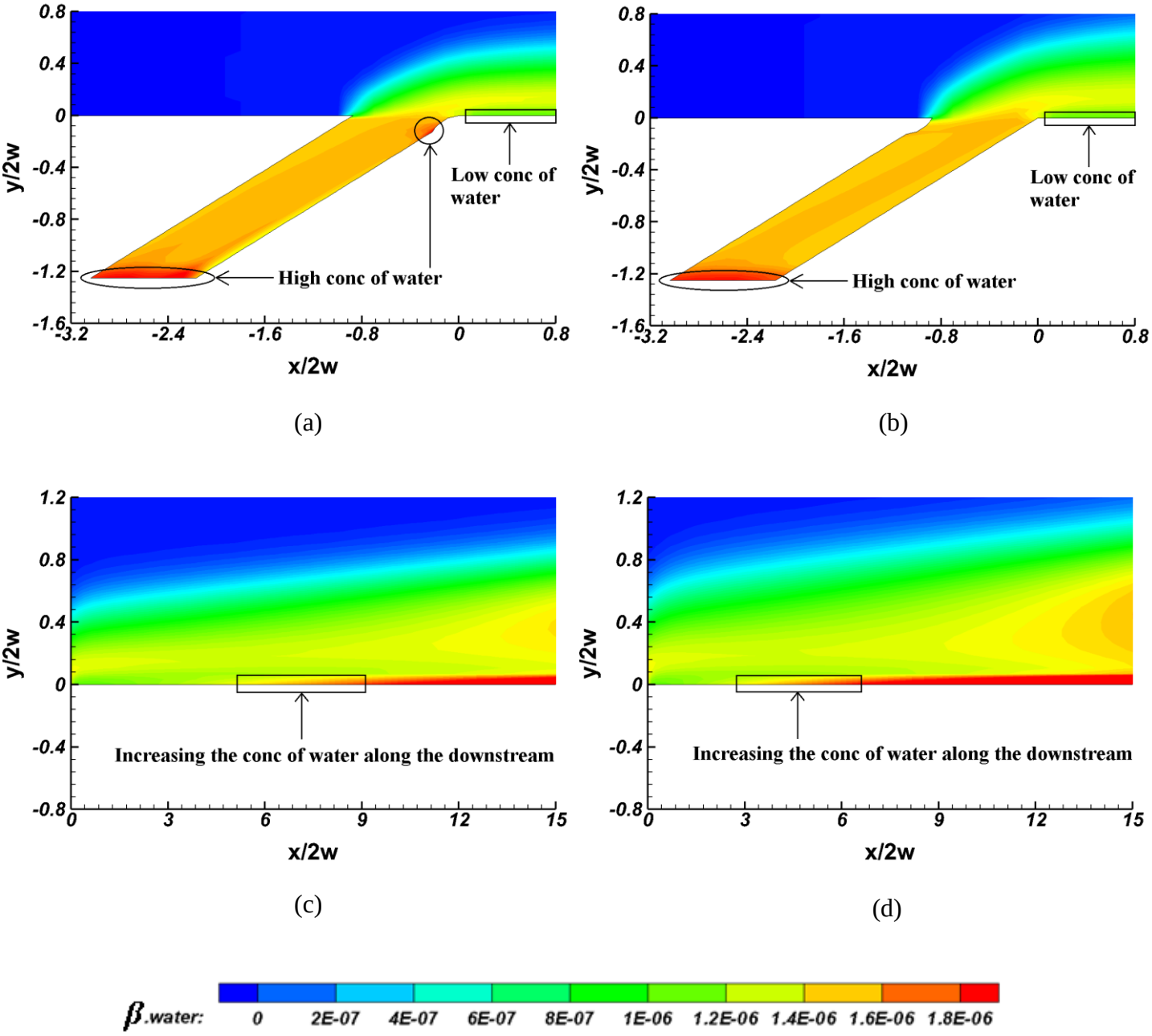

Figure 7. The water concentration at different distances for (a), (c) DL0 and (b), (d) UL0.

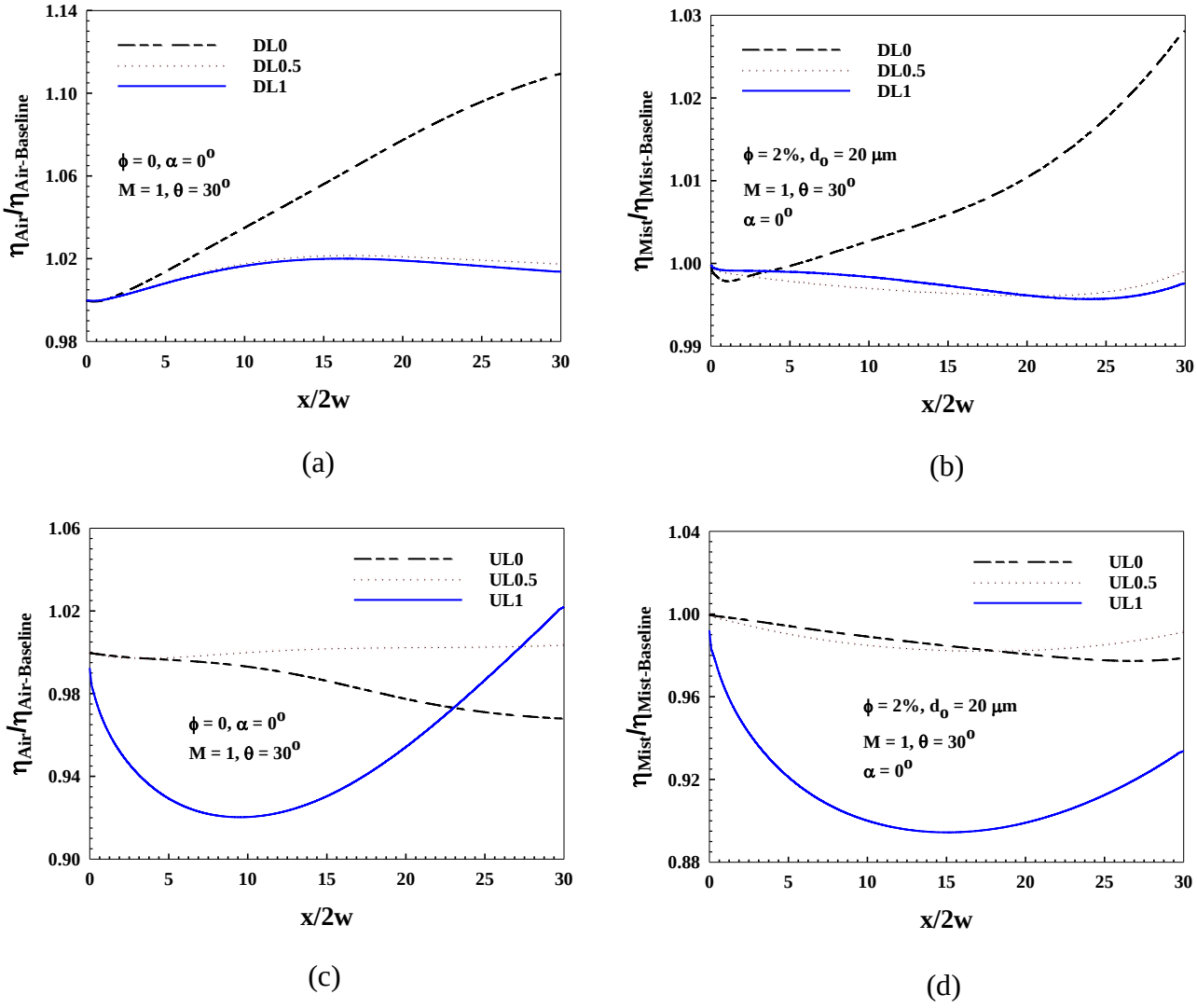

Figure 8. Film cooling effectiveness normalized with the unblocked hole cooling effectiveness for (a) downstream blockage and air injection (b) downstream blockage and mist injection (c) upstream blockage and air injection (d) upstream blockage and mist injection.

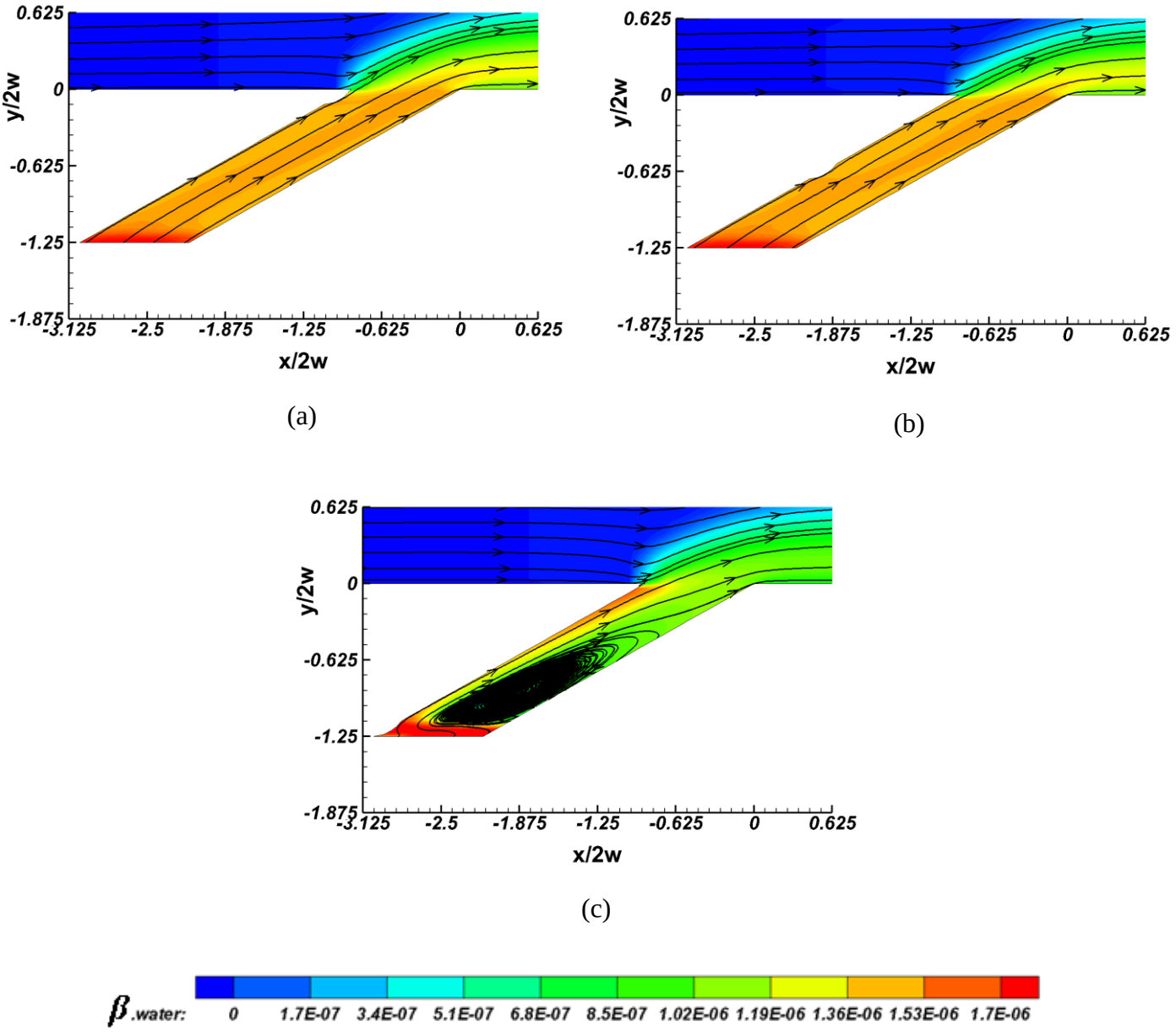

Figure 9. Water volume fraction contours with streamlines at (a) UL0, (b) UL0.5 and (c) UL1.

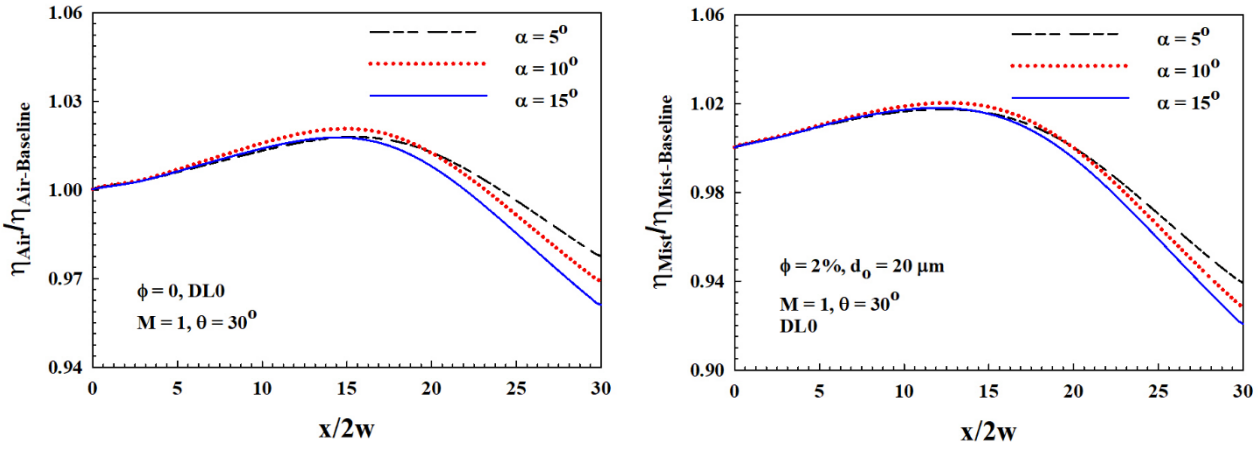

Figure 10. Film cooling effectiveness normalized with the film cooling effectiveness without ramp for (a) air injection (b) mist injection due to hole blockage.

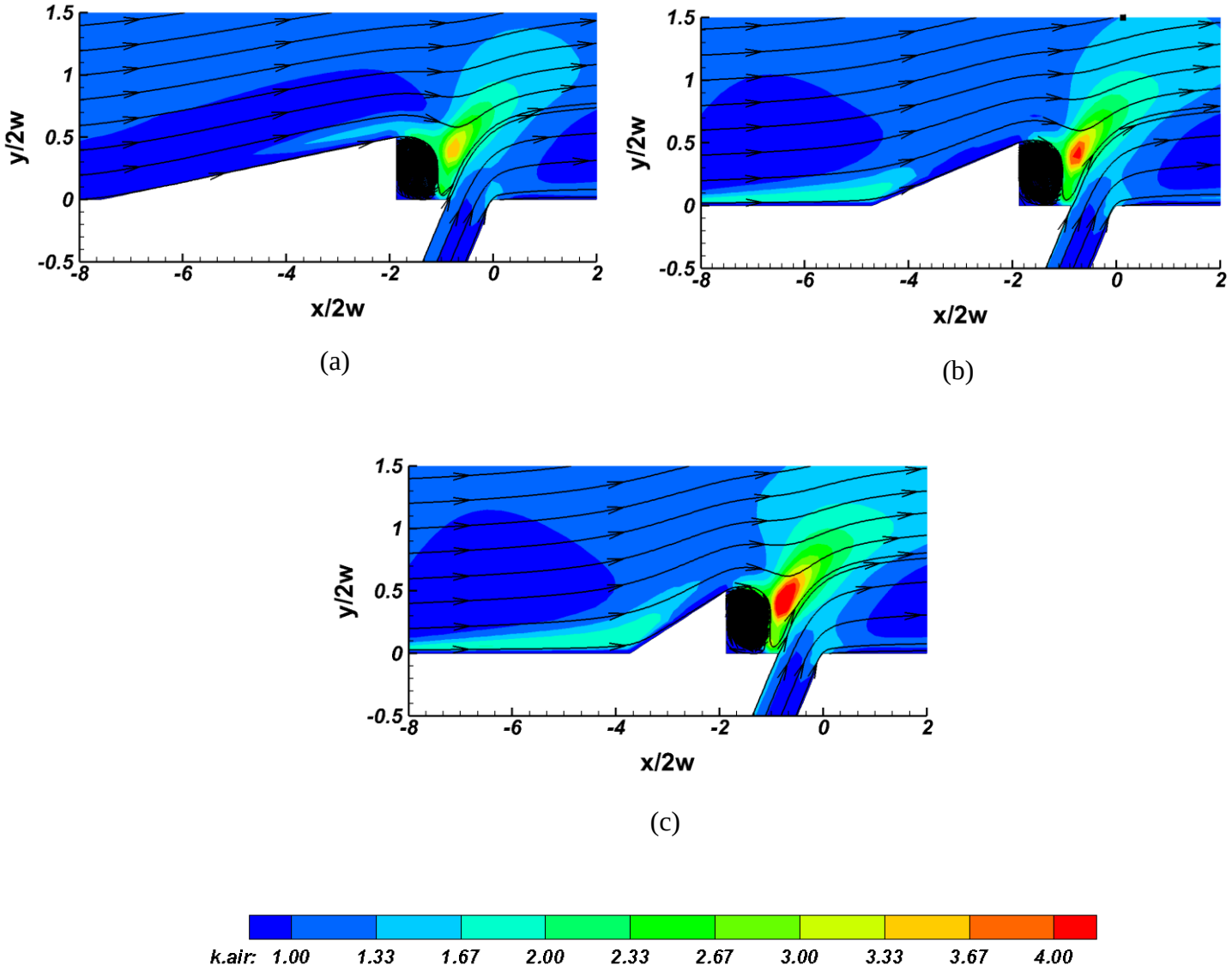

Figure 11. Turbulent kinetic energy at (a) α = 5º, (b) α = 10º and (c) α = 15º.

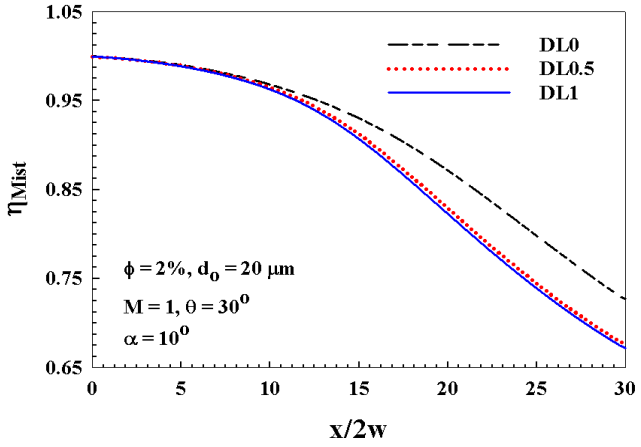

(a)

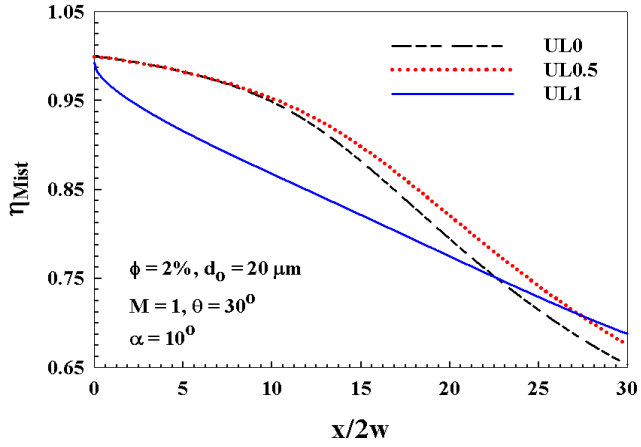

(b)

Figure 12. Mist film cooling effectiveness in the presence of upstream ramp for (a) downstream blockage and (b) upstream blockage.

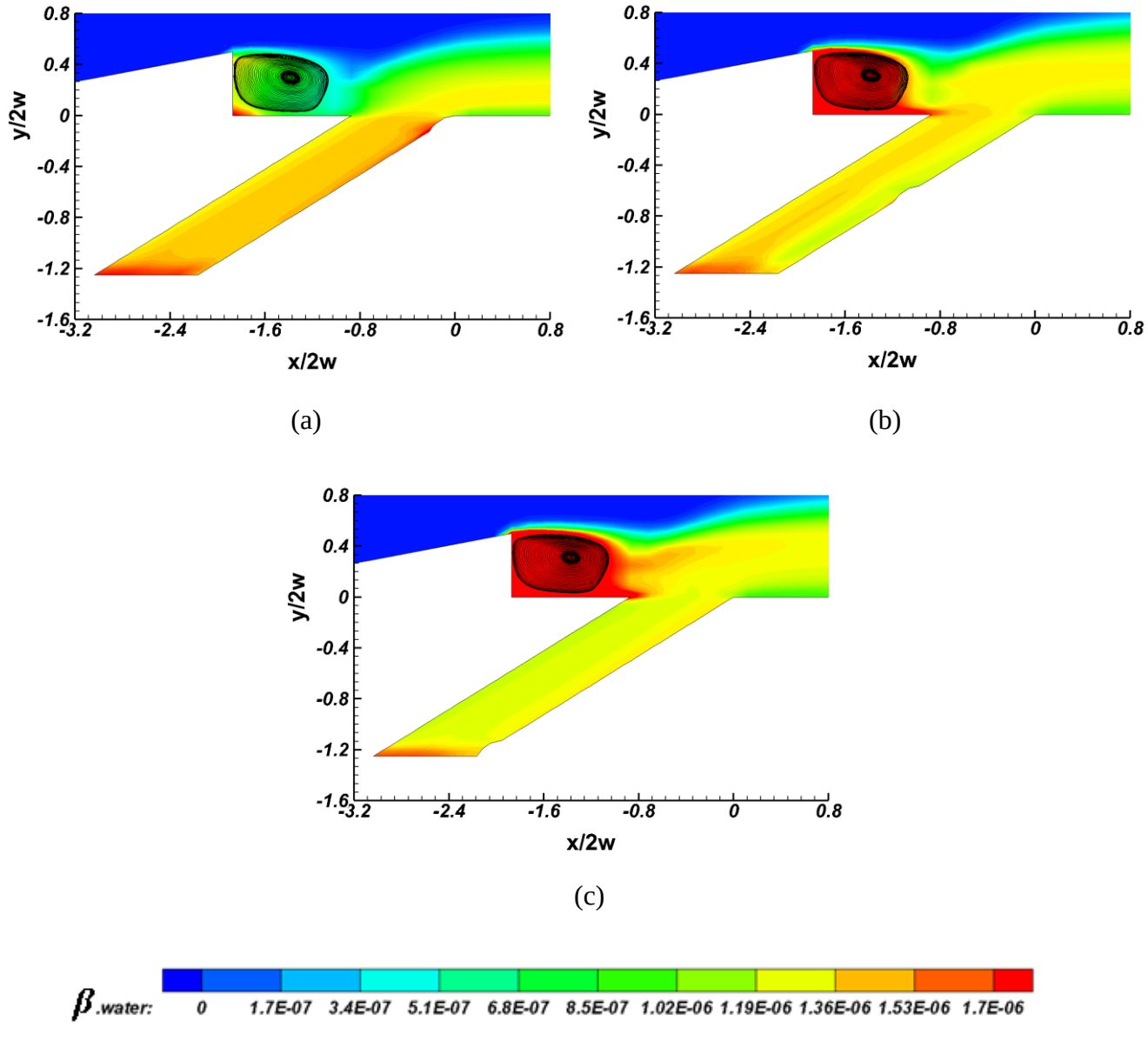

Figure 13. Water enters the recirculation zone due to (a) DL0, (b) DL0.5 and (c) DL1.

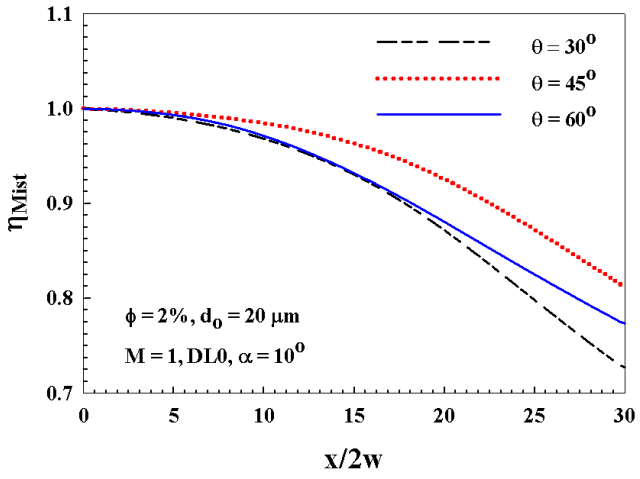

Figure 14. Mist Film cooling effectiveness for various slot angle, θ in the presence of ramp and hole blockage.

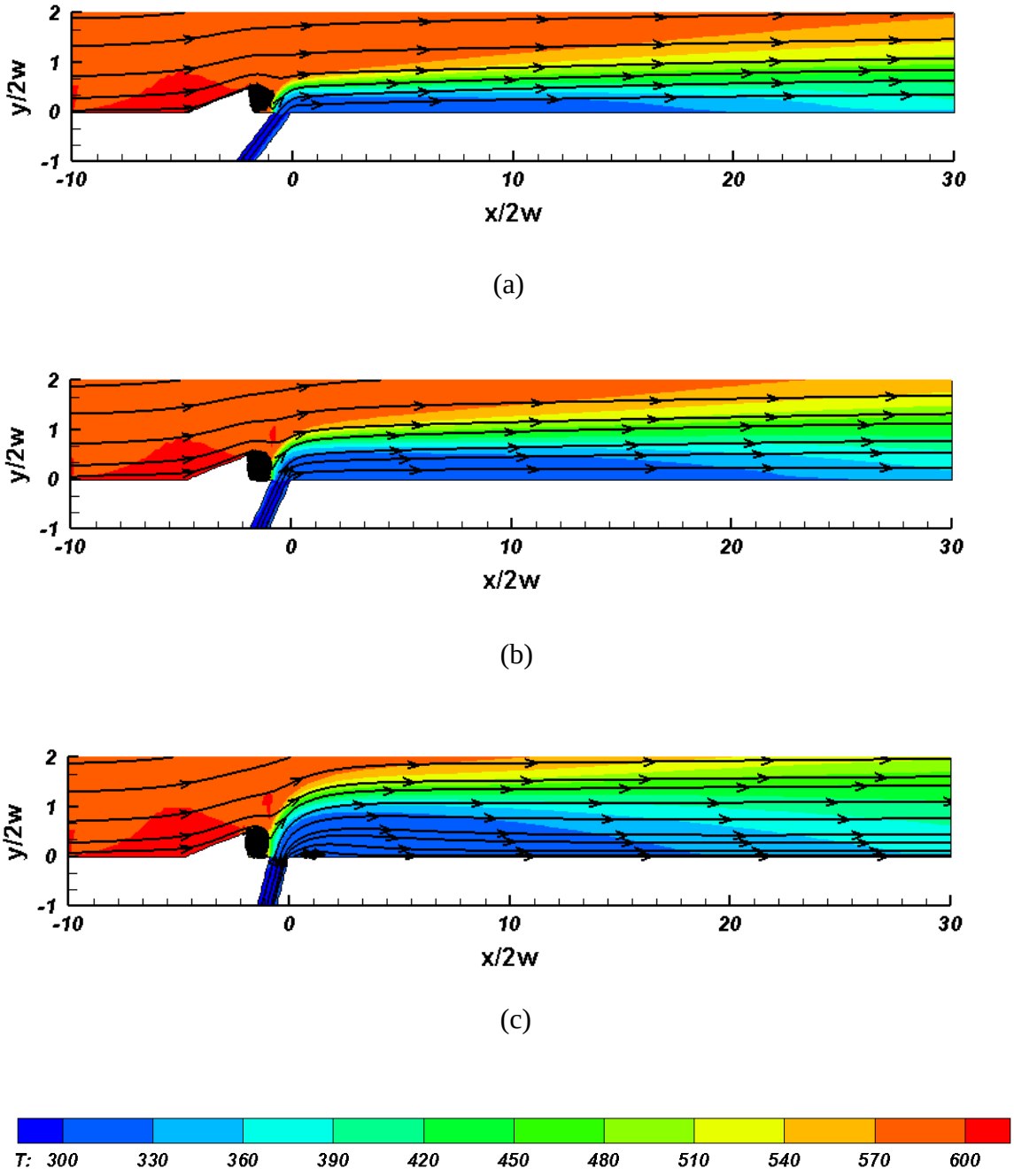

Figure 15. Streamlines and temperature contours at slot angles (a) θ=30º, (b) θ=45º and (c) θ=60º with α=10º and DL0.

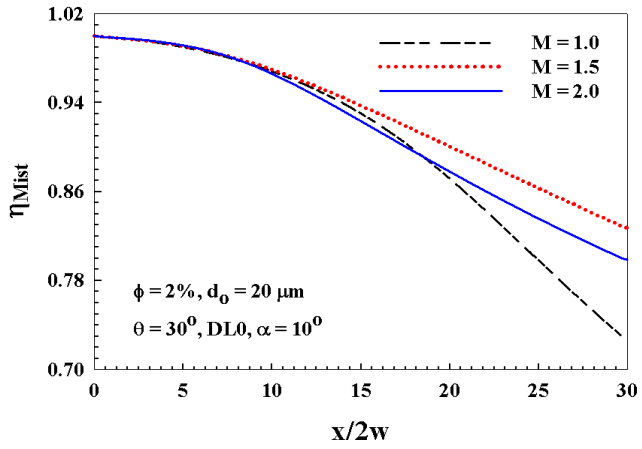

Figure 16. Mist Film cooling effectiveness for various blowing ratio, M in the presence of ramp and hole deposition.

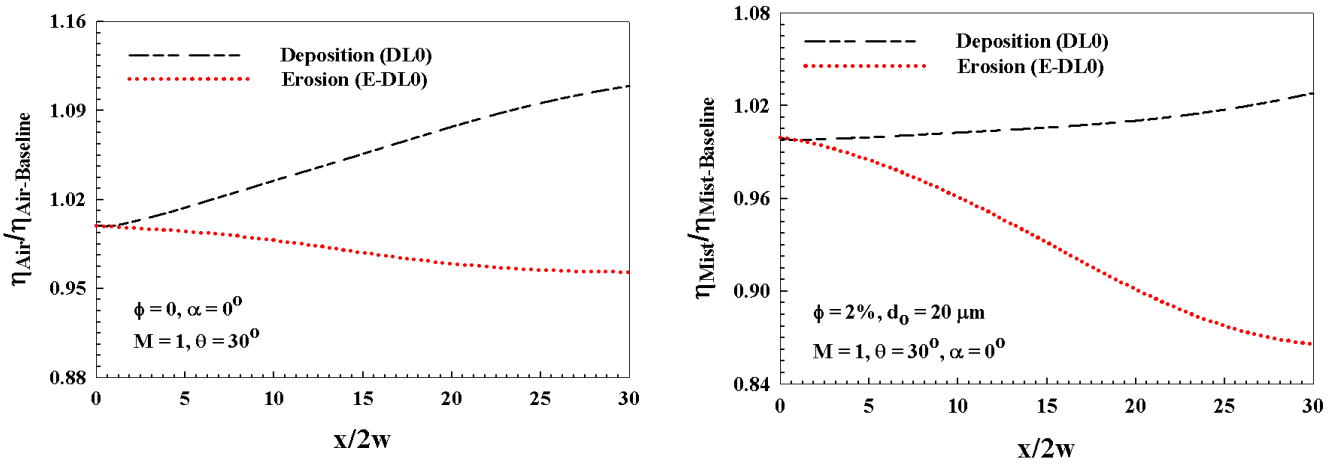

(a) (b)

Figure 17. Film cooling effectiveness normalized with the film cooling effectiveness without hole deposition/erosion for (a) air injection (b) mist injection.

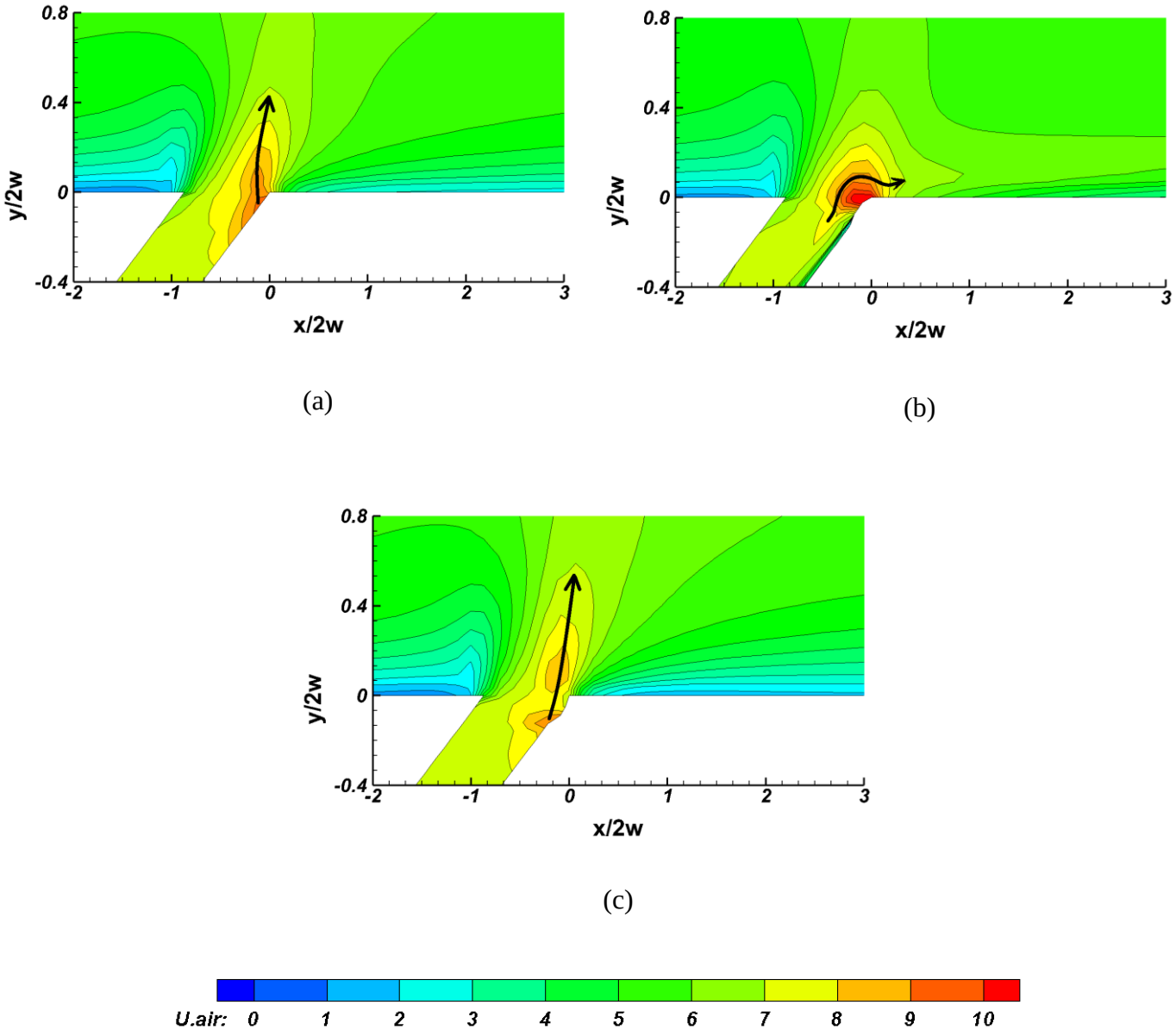

Figure 18. Velocity contours of air for (a) Baseline case (b) DL0 and (c) E-DL0.

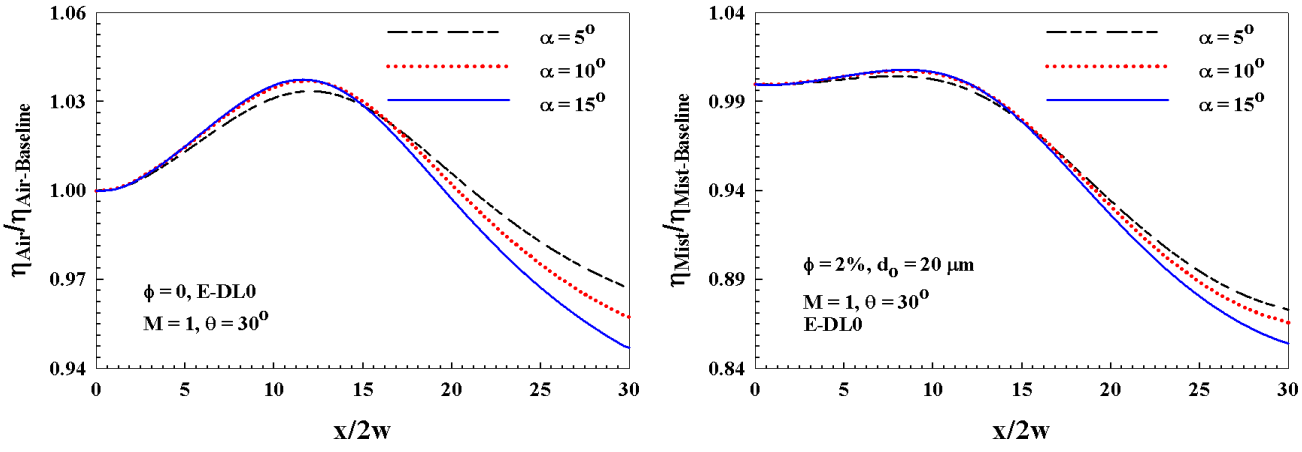

(a) (b)

Figure 19. Film cooling effectiveness normalized with the film cooling effectiveness without ramp for (a) air injection (b) mist injection due to hole erosion.

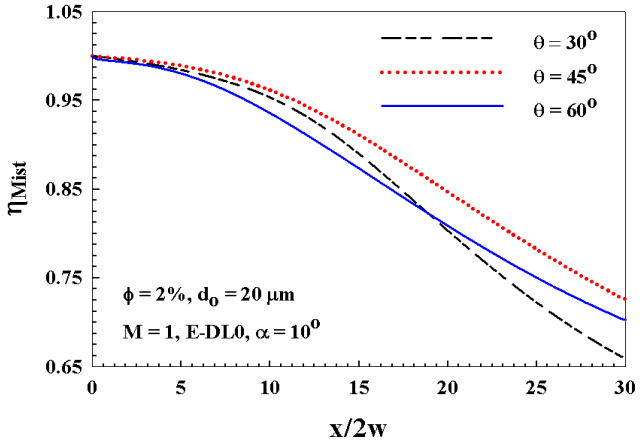

Figure 20. Mist Film cooling effectiveness for various slot angle, θ in the presence of ramp and hole erosion.

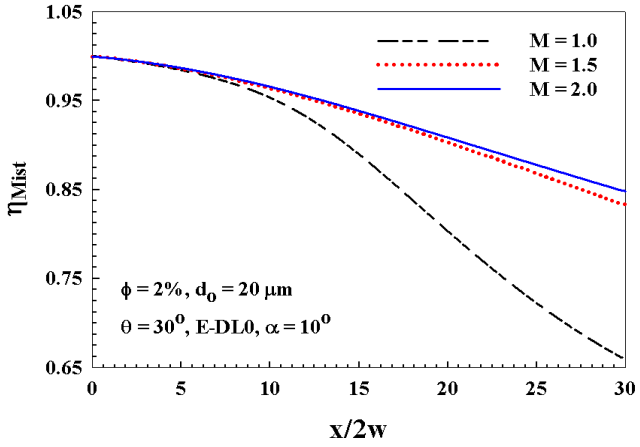

Figure 21. Mist Film cooling effectiveness for various blowing ratio, M in the presence of ramp and hole erosion.